

Absence of logarithmic and algebraic scaling entanglement phases due to skin effect

Xu Feng,^{1,*} Shuo Liu,^{2,*} Shu Chen,^{3,4,5,†} and Wenan Guo^{1,6,‡}

¹*Department of Physics, Beijing Normal University, Beijing 100875, China*

²*Institute for Advanced Study, Tsinghua University, Beijing 100084, China*

³*Beijing National Laboratory for Condensed Matter Physics,*

Institute of Physics, Chinese Academy of Sciences, Beijing 100190, China

⁴*School of Physical Sciences, University of Chinese Academy of Sciences, Beijing 100049, China*

⁵*Yangtze River Delta Physics Research Center, Liyang, Jiangsu 213300, China*

⁶*Beijing Computational Science Research Center, Beijing 100193, China*

(Dated: January 3, 2023)

Measurement-induced phase transition in the presence of competition between projective measurement and random unitary evolution has attracted increasing attention due to the rich phenomenology of entanglement structures. However, in open quantum systems with free fermions, a generalized measurement with conditional feedback can induce skin effect and render the system short-range entangled without any entanglement transition, meaning the system always remains in the “area law” entanglement phase. In this work, we demonstrate that the power-law long-range hopping does not alter the absence of entanglement transition brought on by the measurement-induced skin effect for systems with open boundary conditions. In addition, for the finite-size systems, we discover an algebraic scaling $S(L, L/4) \sim L^{3/2-p}$ when the power-law exponent p of long-range hopping is relatively small. For systems with periodic boundary conditions, we find that the measurement-induced skin effect disappears and observe entanglement phase transitions among “algebraic law”, “logarithmic law”, and “area law” phases.

I. INTRODUCTION

The rich phenomenology of entanglement structures has sparked increased interest in measurement-induced phase transition (MIPT) [1–15]. A prototypical model exhibiting MIPT is the monitored quantum systems undergoing random unitary evolution interspersed by local projective measurements, in which the random unitary evolution tempts to induce large-scale entanglement while the measurements shatter quantum coherence and thereby suppress entanglement growth. Below a critical measurement rate p_c , the entanglement within the system obeys “volume law”. Increasing the measurement rate above the critical rate, the system enters the “area law” entanglement phase [1–4]. Recently, MIPT has also been investigated in the monitored free fermion chain and quantum Ising chain [16–23]. With increasing the rate of the continuous local number measurement, both systems undergo an entanglement transition from the “sub-extensive law” phase into the “area law” phase.

To further understand the nature of the measurement-induced phase transition, the effect of the long-range interaction between qudits (or long-range hopping between free fermions) needs to be considered and remains an essential open question, while the previous studies mainly focus on the monitored systems with local or all-to-all interaction (hopping). In principle, the long-range interaction (hopping) may change the universality class and even induce a richer entanglement phase diagram. For

power-law long-range interacting hybrid quantum circuits, long-range interactions give rise to a continuum of non-conformal universality classes and induce a novel “sub-volume law” phase [24]. Analogously, for monitored power-law hopping free fermion model, long-range hopping induces an unconventional algebraic scaling phase when power-law hopping decay exponent $p \leq d/2 + 1$ where d is spatial dimension [25]. If the power-law long-range interaction is also added, the critical exponent p_c for the algebraic scaling phase will be increased to $d + 1$ [26].

Besides the local measurements, other mechanisms such as non-Hermitian skin effect (NHSE) [27–38] can also suppress entanglement growth and recent work has revealed that the entanglement of free fermion systems undergoing non-Hermitian evolution [39], i.e., the post-selection quantum trajectory without quantum jumps obeys “area law”. Moreover, the suppression effect for entanglement due to skin effect has also been investigated in the presence of quantum jumps, in which the monitored free fermion model includes nearest-neighbor hopping and generalized measurements with conditional feedback. When the measurement rate is non-zero, particles tend to accumulate at one specific edge. The measurement-induced skin effect causes most particles to freeze, rendering the system short-range entangled. Therefore, the entanglement averaged over the full trajectories also obeys “area law”. It is worth noting that the skin effect relies on open boundary conditions (OBCs).

An interesting and vital question is, what are the entanglement behaviors for the free fermion systems with long-range hopping and measurement-induced skin effect? Theoretically, long-range hopping can spread quantum information to particles at any distance, making it

* The two authors contributed equally to this work.

† schen@iphy.ac.cn

‡ wguo@bnu.edu.cn

possible to overcome localization brought on by the skin effect and sustain large-scale entanglement.

To answer this question, we investigate the entanglement behaviors of a monitored free fermion model with power-law long-range hopping and conditional generalized measurement in this work. When periodic boundary conditions (PBCs) are adopted, we find that the skin effect disappears. We obtain an entanglement phase diagram (see Fig. 3(a)) including “area”, “logarithmic” and “algebraic law” phases via tuning the power-law exponent p and the generalized measurement rate γ . Our numerical results are consistent with the previous study in which the generalized measurement is replaced by measurement for local density [25]. While with OBCs, we obtain convincing numerical results in support that the skin effect survives under the power-law long-range hopping. Despite the system ultimately entering the “area law” entanglement phase in the thermodynamics limit (see Fig. 3(b)), we show that finite-size effects can induce different entanglement behaviors via tuning the parameters. When p is large, we find that the entanglement behaviors are similar to the case with nearest hoppings ($p \rightarrow \infty$), and the entanglement decays to zero fastly with the increasing of the system size L [40]. Nevertheless, when p is small, we find an algebraic scaling behavior $S(L, L/4) \sim L^{\frac{3}{2}-p}$ for finite-size system.

The paper is organized as follows. In Sec. II, we introduce the model studied in this work: a monitored free fermion model with power-law long-range hopping and generalized measurement and the observables that quantify the entanglement and the skin effect. Next, in Sec. III, we perform numerical simulations using the quantum jump approach and show the numerical results of different Hamiltonian parameters and boundary conditions. Then we analyze the entanglement entropy, classical entropy, and local density distributions of steady states to show the competition between long-range hopping and the measurement-induced skin effect, thus inferring the phase diagram. Moreover, in Sec. IV, we investigate the case without conditional feedback, in which the numerical results are sensitive to time step δt in quantum jump simulation and observe a “pseudo skin effect” when δt is not small enough. Finally, in Sec. V, we give our conclusions and some outlooks. Technical details about numerical simulation are described in Appendix A. In B, we show more supportive numerical results.

II. MODEL AND MEASUREMENT PROTOCOLS

We consider a one-dimensional (1D) free fermion model with power-law long-range hopping. The Hamiltonian is as follows:

$$\hat{H}_0 = \sum_{i \neq j} \frac{t}{|i-j|^p} \hat{c}_i^\dagger \hat{c}_j, \quad (1)$$

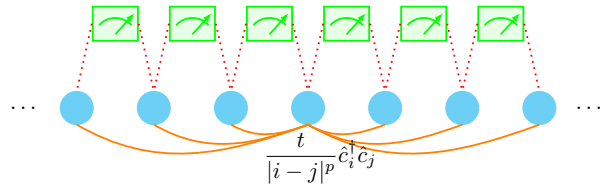


FIG. 1. The schematic diagram for the free fermion model with power-law long-range hopping and generalized continuous measurements. The generalized measurements (green block) act on every pair of neighboring sites.

where \hat{c}_i and \hat{c}_i^\dagger are annihilation and creation operators of the spinless fermion at site i , respectively, t is the hopping strength, and p is the exponent determining the hopping range. We set $t = 1$ throughout the work. To avoid the singular fermion dispersion, we mainly focus on the case $p > 1$ [25].

Different from projective measurements in the hybrid quantum circuits, the continuous measurement process for the free fermion model, which is an open quantum system, is a kind of weak measurement, and the monitoring dynamics is described by the stochastic Schrödinger equation (SSE) [41–45],

$$d|\psi\rangle = -i\hat{H}_{\text{eff}}|\psi\rangle dt + \sum_{\mu} \left[\frac{\hat{L}_{\mu}}{\sqrt{\langle \hat{L}_{\mu}^\dagger \hat{L}_{\mu} \rangle}} - 1 \right] |\psi\rangle dW_{\mu}, \quad (2)$$

where \hat{L}_{μ} is the quantum jump operator modeling the conditional monitored observable, and each dW_{μ} is a discrete, independent Poisson random variable $dW_{\mu} = 0$ or 1, with mean value $\overline{dW_{\mu}} = \gamma \langle \hat{L}_{\mu}^\dagger \hat{L}_{\mu} \rangle dt$ in which γ is the monitoring rate. And the effective Hamiltonian is

$$\hat{H}_{\text{eff}} = \hat{H}_0 - i\frac{\gamma}{2} \sum_{\mu} \hat{L}_{\mu}^\dagger \hat{L}_{\mu}. \quad (3)$$

A. Quantum jump operator

Inspired by [40], we choose the quantum jump operator

$$\hat{L}_i = \hat{U}_i \hat{P}_i = \frac{1}{2} e^{i\theta \hat{n}_{i+1}} \hat{\xi}_i^\dagger \hat{\xi}_i, \quad (4)$$

where unitary feedback $\hat{U}_i = e^{i\theta \hat{n}_{i+1}}$ and measurement operator $\hat{P}_i = \frac{1}{2} \hat{\xi}_i^\dagger \hat{\xi}_i$ with $\hat{\xi}_i^\dagger = \hat{c}_i^\dagger - i\hat{c}_{i+1}^\dagger$. We focus on the case with $\theta = \pi$ firstly, which is more intuitive for measurement-induced skin effect and defer the discussions about the case with $\theta = 0$, i.e., no conditional feedback, to Sec. IV.

Physically, $\hat{\xi}_i^\dagger$ can be regarded as the creation operator of a right-moving quasi-mode. Because $\hat{\xi}_i^\dagger = \sum_k g(k) \hat{c}_k^\dagger$ and $|g(k)|^2 \propto (1 - \sin k)$, consequently $\hat{\xi}_i^\dagger$ induces imbalance particle distributions in momentum space. There-

fore, the current $J = \int_{-\pi}^{\pi} v_k n_k$, where v_k for small monitoring rate γ can be approximated as power-law hopping free fermion case $v_k = \partial_k E(k) = -2 \sum_m m \sin(mk)/m^p$, is positive, which indicates the right moving quasi-mode. The conditional feedback \hat{U}_i is for converting the right-moving quasi-mode $\hat{\xi}_i^\dagger = \hat{c}_i^\dagger - i\hat{c}_{i+1}^\dagger$ into left-moving quasi-mode $\hat{\xi}_i^{\prime\dagger} = \hat{c}_i^\dagger + i\hat{c}_{i+1}^\dagger$ ($|g(k)|^2 \propto (1 + \sin k)$). Past research shows that for the nearest hopping case, the conditional feedback is indispensable for measurement-induced skin effect; otherwise, the right-moving quasi-mode created by quantum jumps is canceled by the left-moving quasi mode induced by \hat{H}'_{eff} . In fact, there is huge freedom to choose θ . However, the numerical results reveal that with the decrease of θ/π , the fluctuation of the boundary between occupied and unoccupied regions gets extended until the measurement-induced skin effect can not be observed in the $\theta \rightarrow 0$ limit. More details and discussions can be found in Ref. [40].

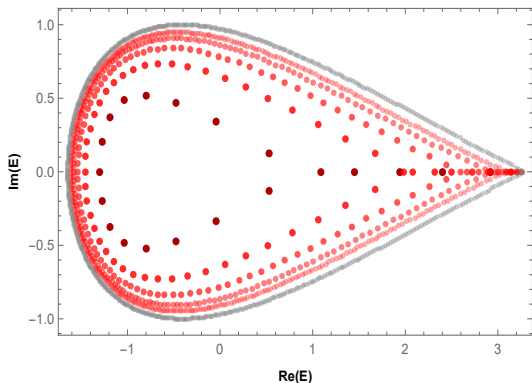


FIG. 2. Energy spectrum of \hat{H}'_{eff} with $p = 2.0$, $\gamma = 2.0$, and $L = 20, 50, 100, 200, 400$ under OBC. Dark (light) color corresponds to small (large) system size L , and the OBC spectrum approaches the PBC spectrum (Gray) as L increases.

B. The effective Hamiltonian \hat{H}'_{eff}

The effective non-Hermitian Hamiltonian \hat{H}'_{eff} is

$$\hat{H}'_{\text{eff}} = \sum_{i \neq j} \frac{t}{|i-j|^p} \hat{c}_i^\dagger \hat{c}_j + \frac{\gamma}{4} \sum_i (\hat{c}_i^\dagger \hat{c}_{i+1} - \hat{c}_{i+1}^\dagger \hat{c}_i - i(\hat{n}_i + \hat{n}_{i+1})). \quad (5)$$

Since overall dissipation only gives a shift to the spectrum, we will directly analyze \hat{H}'_{eff} 's energy spectrum, where

$$\hat{H}'_{\text{eff}} = \sum_{i \neq j} \frac{t}{|i-j|^p} \hat{c}_i^\dagger \hat{c}_j + \frac{\gamma}{4} \sum_i (\hat{c}_i^\dagger \hat{c}_{i+1} - \hat{c}_{i+1}^\dagger \hat{c}_i). \quad (6)$$

As shown in Fig. 2, for small system size L , the OBC eigenstates are clearly distinct from PBC eigenstates.

However, with the increase of L , the OBC energy spectrum approaches the PBC energy spectrum gradually.

We now discuss \hat{H}'_{eff} 's single-particle OBC eigenstates. In the $p \rightarrow \infty$ limit, it is exactly the Hatano-Nelson model [46]. The magnitude of the single-particle OBC eigenstates exponentially decays with size-independent localization length. While for $p = 0$, i.e., the all-to-all limit, there is almost no difference between PBC and OBC, and NHSE is absent.

Beyond the single-particle case, for the Hatano-Nelson model ($p = \infty$), the density imbalance between two half sides grows linearly with the system size L , i.e., the skin effect still exists for many-body systems [47]. However, when p is finite, it's reasonable to anticipate that the density imbalance grows more slowly with L or even saturates for large L , i.e., the skin effect may be suppressed or destroyed by long-range hopping. Worth to mention for any $\gamma > 0$, skin modes induced by \hat{H}'_{eff} tend to localize at the left side.

The conditional feedback is necessary for measurement-induced skin effect when $p = \infty$ [40]. Otherwise, the quasi-modes with opposite directions induced by the quantum jump and \hat{H}'_{eff} will probably cancel each other. When the skin effect emerges, due to the Pauli exclusion principle, most of the particles will freeze, thus suppressing the quantum correlation developed by hopping and leading to “area law” entanglement [40]. It is worth noting that the measurement-induced skin effect only can be revealed with OBC. To demonstrate the different entanglement behaviors caused by the boundary conditions, both cases with PBC and OBC are investigated in this work.

C. Observables

Firstly, to quantify the strength of the skin effect, we introduce

$$\Delta n = |N_{\text{left}} - N_{\text{right}}|/N_{\text{tot}}, \quad (7)$$

where N_{left} (N_{right}) represents the number of particles in the left (right) half side, and N_{tot} means the total particle number. For strong skin effect, particles almost accumulate at one side, thus $\Delta n \approx 1$. While if density distribution is uniform, $\Delta n \approx 0$.

Since both the \hat{H}'_{eff} and monitoring operator \hat{L}_μ are quadratic, the dynamical evolution preserves gaussianity with a Gaussian initial state. For the Gaussian state, the bipartite entanglement entropy with subsystem $A = [1, L/4]$ is given by [48–52]

$$S(L, L/4) = \sum_{i=1}^{L/4} s(\lambda_i), \quad (8)$$

$$s(\lambda_i) = -\lambda_i \log \lambda_i - (1 - \lambda_i) \log (1 - \lambda_i),$$

where λ_i are eigenvalues of sub-correlation matrix $G_{m,n}^A = \langle c_m^\dagger c_n \rangle$, $m, n \in A$.

Another quantity to characterize the strength of the skin effect is classical entropy [40],

$$S_{\text{cl}} = - \sum_{i=1}^L [\langle n_i \rangle \log \langle n_i \rangle + (1 - \langle n_i \rangle) \log (1 - \langle n_i \rangle)], \quad (9)$$

where $\langle n_i \rangle$ is the expectation value of particle number on site i which can be obtained from the i -th diagonal elements of the correlation matrix $G_{i,i} = \langle \hat{c}_i^\dagger c_i \rangle$. In addition, S_{cl} is an upper bound of bipartite entanglement entropy. Due to the subadditivity of bipartite entanglement entropy [53, 54], the entanglement entropy of subsystem A satisfies the following inequation

$$S_A = \frac{1}{2}(S_A + S_B) \leq \frac{1}{2} \sum_i S_i, \quad (10)$$

where B is the complementary subsystem with A , and S_i is entanglement entropy of site i . In general, $\sum_i S_i \leq S_{\text{cl}}$. Therefore, the entanglement entropy $S(L, L/4)$ is bounded by half of S_{cl} . In this work, we focus on the half-filling case with the particle number $N = L/2$, and the evolution described by SSE respects $U(1)$ symmetry, i.e., the particle number is conserved. With strong skin effect, about one-half of sites are occupied and one-half unoccupied (see Fig. S3), so apparently $S_{\text{cl}} \sim O(1)$ and thus S_{cl} is independent of system size L . By contrast, in the absence of the skin effect, $S_{\text{cl}} \sim O(L)$.

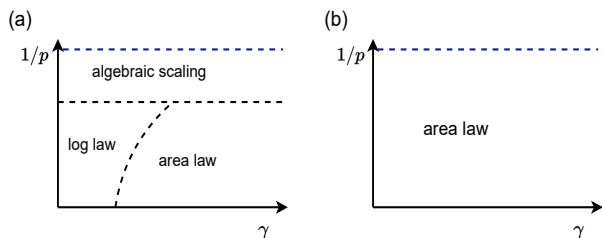


FIG. 3. Schematic phase diagram for $p > 1$ (blue dotted line corresponds to $p = 1$) and $\gamma > 0$. (a) There are three phases: “logarithmic law”, “area law,” and “algebraic scaling” phases (PBC). (b) The entanglement is suppressed by measurement-induced skin effect and obeys “area law” (OBC).

III. NUMERICAL RESULTS AND PHASE DIAGRAM

The model proposed above has two tunable parameters. One is monitoring rate γ , which controls the strength of unidirectional particle flows, i.e., the measurement-induced skin effect, caused by \hat{H}_{eff} and quantum jumps. For OBCs, the measurement-induced skin effect is robust against the relatively short-range hopping and nearest interaction [40]. Then Pauli exclusion principle freezes almost all particles, leaving fluctuations in a small region around the boundary of the occupied and unoccupied region (Fig. 4(b)). While for PBCs,

particles flow around the bulk, and thus no skin effect appears (Fig. 4(a)). Via changing boundary conditions, we can explore the role of the skin effect. The other tunable parameter is the hopping decay exponent p . With decreasing of p , the hopping range gets extended. In principle, long enough hopping will weaken or even eliminate the skin effect. Via tuning γ and p with OBC, we can see the competition between skin effect and long-range hopping. It’s worth noting that the generalized measurement is followed by conditional feedback, and we choose $\theta = \pi$ for simplicity in the whole Sec. III.

A. Skin effect induced area law

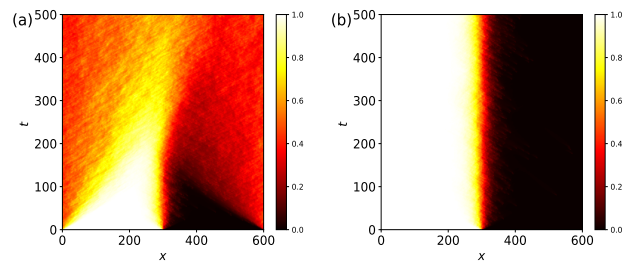


FIG. 4. Density distribution evolution with time for $p = 2.0, \gamma = 0.1$. The initial state is chosen as $|111..000\rangle$. (a) PBC, no skin effect, particle number distribution of steady-state tends to be uniform. (b) OBC, with skin effect, steady state is almost half occupied and half unoccupied.

From the local density distribution, as shown in Fig. 4, the measurement-induced skin effect under OBC can be observed. When the fluctuation region is comparable with the system size, there exists quantum correlations between subsystems A and B , and the bipartite entanglement entropy is finite. However, as the system size increases, subsystem A is far away from the middle fluctuation zone, and the particles in A are completely frozen, which greatly suppresses the entanglement. Therefore, when L is larger than a threshold L_0 , we can see that the entanglement entropy decay to zero fastly with increasing L as shown in Fig. 5. This measurement-induced skin effect that suppresses the entanglement can be enhanced by more frequent generalized measurement (larger γ) and shorter range hopping (larger p) as shown in Fig. 5(a)(b) and Fig. 8(a)(b).

On the other hand, under PBCs, the skin effect disappears, and the local density distribution is uniform when the system reaches the steady state, as shown in Fig. 4(a). The entanglement entropy clearly shows the entanglement phase transition from the “logarithmic law” phase into the “area law” phase with the increase of measurement rate γ as shown in Fig. 5(c)(d), which is consistent with the previous studies [17, 25].

Based on the numerical results discussed above, we conclude that the skin effect will survive and induce the

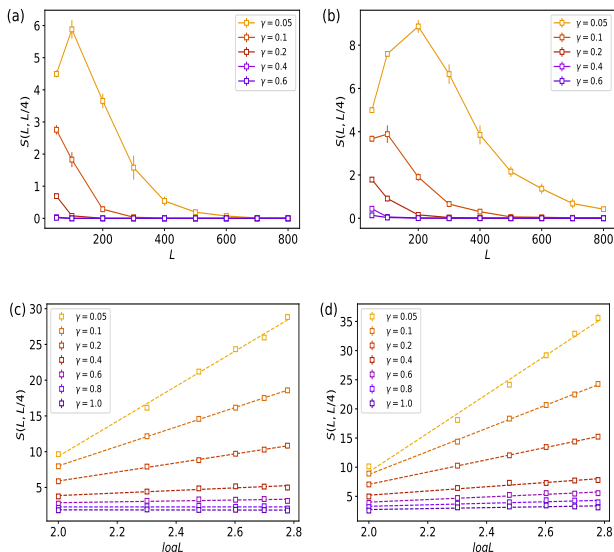


FIG. 5. Entanglement entropy $S(L, L/4)$. (a) OBC, $p = 5.0$ (b) OBC, $p = 2.0$. In both (a) and (b), $S(L, L/4)$ decays to zero, showing the “area law” behavior. (c) PBC, $p = 5.0$ (d) PBC, $p = 2.0$. In both (c) and (d), for small γ , $S(L, L/4)$ follows the “logarithmic law”; for large γ , it follows the “area law”.

“area law” entanglement phase with relatively long-range hopping ($p \geq 2.0$) and monitoring rate $\gamma \geq 0.05$. In the next subsection, we will draw the same conclusions from the scaling relation of the classical entropy S_{cl} and further get some intuition for the case $1 < p < 2.0$ and $\gamma \rightarrow 0$.

B. Scaling behavior of S_{cl}

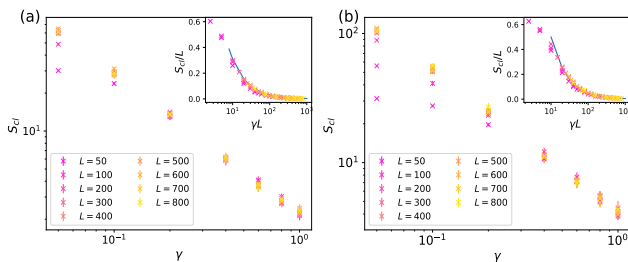


FIG. 6. Classical entropy S_{cl} versus γ on the log-log scale for different system sizes. (a) $p = 5.0$, the blue curve in the inset shows the fit $y = 3.1/x$ for large γL . (b) $p = 2.0$, the blue curve in the inset is the fit $y = 5/x$ for large γL . The scaling relation tells that, even for small γ , S_{cl} behaves as $S_{cl} \propto 1/\gamma$ in the thermodynamics limit.

To further demonstrate the area law phase at OBCs for any $\gamma > 0$, we study the finite-size scaling behavior of the classical entropy $S_{cl}(L)$.

As illustrated in the insets of Fig. 6 (a) and (b) for large $p \geq 2.0$, we find the finite-size scaling relation pro-

posed in [40]

$$S_{cl}(L) = Lf(\gamma L), \quad (11)$$

still holds well for a large range of p we calculated.

In the limit $\gamma \rightarrow 0$ and finite L , this relation holds with $f(0)$ a constant, considering the extension of S_{cl} . Physically, for γ bigger than a threshold γ_0 , the skin effect is so strong that the size of fluctuation areas is stabilized (about $O(1)$) for medium system size ($L \sim 10^2$). Therefore, one expects that $S_{cl}(L)$ be invariant with system size L , as $L \rightarrow \infty$. The scaling Eq. (11) then requires the scaling function $f(\gamma L) \propto 1/(\gamma L)$ as $\gamma L \rightarrow \infty$, which is consistent with the fits for large γL shown in the insets of Fig. 6. Hence, in the thermodynamics limit, for $\gamma > 0$, $S_{cl}(\gamma, L \rightarrow \infty) \propto 1/\gamma$. Therefore, for any nonzero γ , the entanglement entropy is bounded in the thermodynamics limit, and the system enters the “area law” entanglement phase immediately in the presence of generalized measurement ($\gamma > 0$).

Worth to mention numerical results show that the threshold γ_0 increases as p lowers down (see Fig. 6 and Fig. 7). When p is close to 1, the threshold γ_0 gets so big and beyond our numerical capabilities. For example, as Fig. 7(c), (d) show, in the range of γ we calculated, when $p = 1.5$ and $p = 1.1$, $S_{cl}(L)$ does not collapse well for system sizes $L \leq 800$. However, there is a clear tendency that for bigger γ , although beyond our numerical abilities, $S_{cl}(L)$ for various system sizes L will ultimately collapse. Moreover, according to the data collapse in the inset of Fig. 7 (c), (d), we see Eq. (11) is still satisfied, and for $\gamma L \rightarrow \infty$, $f(\gamma L)$ tends to behave as $1/\gamma L$ like in Fig. 6, which means in the thermodynamical limit, $S_{cl} \propto 1/\gamma$.

The behaviors of S_{cl} for different p are consistent with Δn . As shown in Fig. 8, when $p = 2.0, 5.0$, for moderate γ and medium size L , Δn is close to 1, which means particles almost completely localize at the left side, thus S_{cl} should be independent of L and data of S_{cl} for various sizes collapse well. While for $p = 1.1$, even for $L = 800$ and $\gamma = 3.0$, Δn is still not close to 1, which means S_{cl} will be dependent on L and data of S_{cl} for various sizes collapse badly. However, according to Fig. 8, it’s also reasonable to predict for larger L and bigger γ , Δn will finally close to 1, thus $S_{cl} \sim O(1)$. Therefore, for $\gamma L \rightarrow \infty$, $S_{cl} \propto 1/\gamma$ always holds.

The increase of threshold γ_0 is also observed for the nearest hopping case ($p = \infty$) [40]. By changing the θ of the unitary feedback phase factor, it was found that when θ decreases, the threshold γ_0 increases [40]. This is understandable since the decrease of θ and p weakens the skin effect and extends the fluctuation areas. Therefore, one needs bigger γ , namely more frequent measurements to strengthen the skin effect and reduce fluctuation areas.

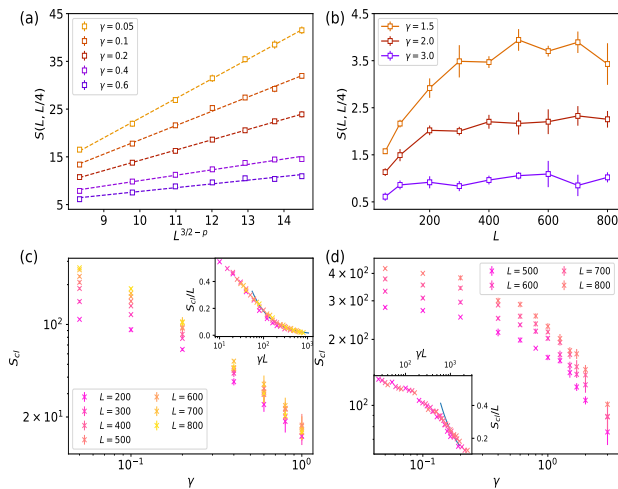


FIG. 7. Entanglement entropy and classical entropy. (a) $p = 1.1$, for small γ and medium size ($L \sim 10^2$), entanglement entropy $S(L, L/4)$ fits well with $L^{3/2-p}$. (b) $p = 1.1$, for large γ , $S(L, L/4)$ quickly saturates. (c) Classical entropy S_{cl} and its data collapse for $p = 1.5$. The blue fitting curve for large γL in the inset is $y = 18/x$. (d) Classical entropy S_{cl} and its data collapse for $p = 1.1$. The blue fitting curve for large γL in the inset is $y = 250/x$.

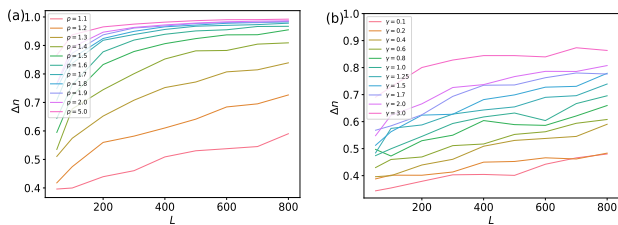


FIG. 8. The imbalance of the particle number distributions between the left and right half side. (a) $\gamma = 0.4$, with the decrease of hopping decay exponent p , Δn decreases, skin effect gets weaker. While with the increase of system size L , Δn grows, namely skin effect gets stronger. (b) $p = 1.1$, with the increase of monitoring rate γ and system size L , Δn grows and skin effect gets strengthened.

C. Finite-size algebraic scaling

It's known that, for $p \geq 2.0$ and nonzero γ , the skin effect already dominates for medium system size ($L \sim 10^2$). Further decreasing p , we find that long-range hopping effects emerge at least for medium system size ($L \sim 10^2$) when both p and γ are relatively small. Take $p = 1.1$ as an example, as shown in Fig. 7(a), for small γ and system sizes L up to 800, although the skin effect reduces the entanglement overall, the entanglement entropy $S(L, L/4)$ seems to scale as $L^{3/2-p}$, similar to what found in [25]. However, this algebraic scaling behavior is a finite-size effect.

In the following, we will support our viewpoint from two aspects. The first aspect is about particle num-

ber distributions. For medium size systems ($L \sim 10^2$), the entanglement entropy is mainly contributed from the middle fluctuation area, which is comparable with system size L due to long-range hopping. However, with the increase of L , the size of the fluctuation zone narrows down with respect to system size L (see Fig. S2). This is consistent with Fig. 8(b). With the increase of L , the proportion of particles in the left half side grows, and the skin effect strengthens. So in the thermodynamics limit, it's reasonable to argue that the fluctuation areas are in the order of $O(1)$ size; thus, the entanglement entropy will saturate. The second aspect is from the scaling behavior Eq. (11) of $S_{cl}(L)$. As discussed in the previous subsection, even for $p \rightarrow 1$, the classical entropy $S_{cl}(\gamma)$ still behaves as $1/\gamma$ for any nonzero γ in the thermodynamic limit, so the entanglement entropy should be bounded. Therefore, based on these two aspects, the algebraic scaling behavior should disappear in the thermodynamic limit.

Indeed, when the monitoring rate γ is big, as shown in Fig. 7(b), the entanglement entropy quickly saturates with L . These entanglement entropy behaviors are also in agreement with particle number distributions. As shown in Fig. 9(a) and 9(b), at $p = 1.1$, for small γ , the skin effect is weak, the quantum correlation zone is comparable with system size; thus finite-size algebraic scaling behaviors emerge. While for large γ , unidirectional flow increases, thus the skin effect gets strengthened, which greatly suppresses entanglement growth.

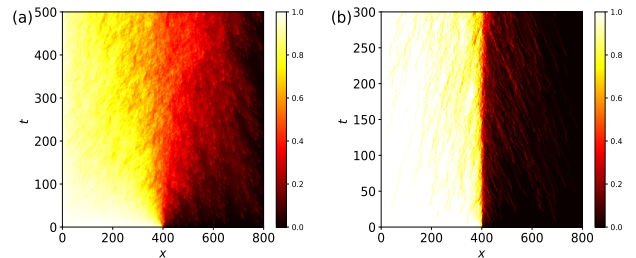


FIG. 9. Density distribution evolution with time for $p = 1.1$ and $L = 800$ under OBCs, the initial state is chosen as $|111..000\rangle$. (a) $\gamma = 0.1$, skin effect is weak. Quantum correlation is developed in the middle zone ($\sim O(L)$ size). (b) $\gamma = 3.0$, skin effect is strong.

So the “logarithmic law” and “algebraic law” phases are absent due to the skin effect and leaving only the “area law” phase. In other words, power-law hopping with exponent $p > 1$ improves the size of fluctuation areas and weakens the skin effect but can not completely eliminate the skin effect. Therefore, in the thermodynamic limit, the skin effect will always dominate, thus induce “area law” phase.

The schematic phase diagrams for PBCs and OBCs are depicted in Fig. 3. For the PBCs, the phase diagram is consistent with previous results [25], in which the “observer” continuously measures the local particle density.

Theoretically, for $p \leq 3/2$ ($p \geq 3/2$), the long-range hopping is relevant (irrelevant), which is reflected on the first-order RG equation [25]. Therefore, for $p \leq 3/2$, frequent local measurements cannot overcome the entanglement generated by long-range hopping. This theoretical analysis also fits the PBCs case here since the measurements in our model only include local density measurement and nearest hopping; thus, the long-range hopping shall still dominate for $p \leq 3/2$. However, the analysis breaks down for the OBCs due to the skin effect. Because most particles tend to localize at one side and be next to each other under OBCs, the Pauli exclusion principle hinders long-range hopping. Therefore, even for $p \leq 3/2$, the long-range hopping is suppressed, leading to the “area law” phase.

IV. NO-FEEDBACK CASE

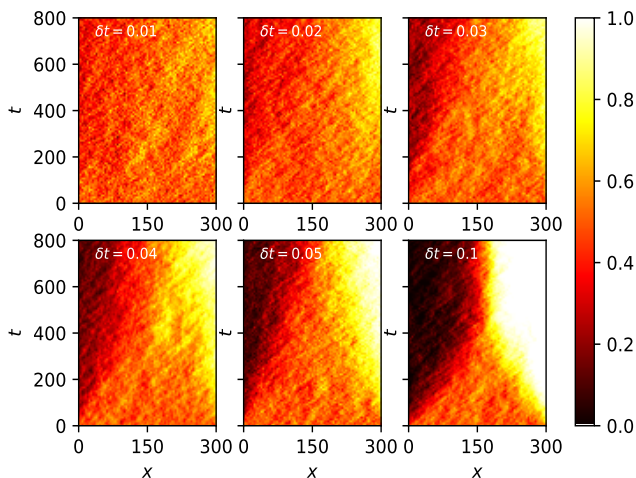


FIG. 10. Density distribution evolution with time under OBCs for the no-feedback case with $\gamma = 2.0$, $p = 2.0$, $L = 300$. The initial state is $|1010\dots10\rangle$. The six subfigures correspond to time step $\delta t = 0.01, 0.02, 0.03, 0.04, 0.05, 0.1$. When δt is small enough, there is no skin effect; while increasing δt , the “pseudo skin effect” emerges.

The previous section (Sec. III) focuses on the case with conditional feedback ($\theta = \pi$). Here, we will investigate no conditional feedback case ($\theta = 0$) briefly. It’s known that the density matrix, which can be acquired through averaging over all measurement outcomes (trajectories), evolves according to the Lindblad master equation [45, 55]

$$\frac{d\hat{\rho}}{dt} = -i [\hat{H}, \hat{\rho}] + \gamma \sum_{\alpha} (\hat{L}_{\alpha} \hat{\rho} \hat{L}_{\alpha}^{\dagger} - \frac{1}{2} \{ \hat{L}_{\alpha}^{\dagger} \hat{L}_{\alpha}, \hat{\rho} \}). \quad (12)$$

For no-feedback case, the Lindblad operator $\hat{L}_i = \frac{1}{2} \hat{\xi}_i^{\dagger} \hat{\xi}_i$ is Hermitian. Apparently, the steady state is the maximally mixed state $\rho_{ss} \sim \mathbb{I}$, thus the particle distribution

is uniform since the number operator \hat{n}_i is linear. Therefore, there is no skin effect for the no-feedback case, and theoretically, we can observe MIPT for the no-feedback case under OBCs. However, numerically we find the quantum jump simulation method is sensitive to time step δt for the no-feedback case when γ is relatively large. As Fig. 10 shows, with the increase of δt , the “pseudo skin effect” emerges and destroys MIPT.

This phenomenon is also verified in particle current J under PBCs, with J defined as

$$J = \frac{i}{L} \sum_{n=1}^L (\langle \hat{c}_n^{\dagger} \hat{c}_{n+1} \rangle - \langle \hat{c}_{n+1}^{\dagger} \hat{c}_n \rangle). \quad (13)$$

Similar to the previous study of NHSE and Liouvillian skin effect [29, 56], the nonzero PBC current means that the skin effect exists under OBCs. As demonstrated in Fig. 11, for $p = 2.0$, $\gamma = 2.0$, $L = 300$, when δt is not small enough, such as $\delta t = 0.05$, the current J is finite, and skin effect seems to emerge under OBCs. However, with the decrease of δt , the current J vanishes. Therefore, there must be no skin effect in the continuous measurement limit for the no-feedback case, which is in agreement with the intuition from the Lindblad master equation. Theoretically, the errors caused by finite δt are the consequences of utilizing the first-order approximation of $\gamma \delta t$ to effectively simulate continuous measurements. Therefore, we must carefully select sufficiently small δt for big monitoring rate γ to avoid the “pseudo skin effect”.

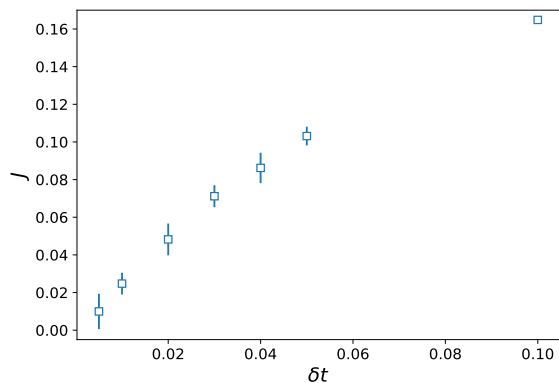


FIG. 11. The current J under PBCs for the no-feedback case with $p = 2.0$, $\gamma = 2.0$, $L = 300$. With the decrease of simulation time step δt , current J decays to zero, which means that there is no skin effect in the continuous measurement limit $\delta t \rightarrow 0$.

V. CONCLUSION AND OUTLOOK

In this paper, we proposed a monitored power-law long-range hopping free fermion model with generalized measurement and conditional feedback. Based on convincing numerical results, we have demonstrated that the

measurement-induced skin effect (with OBCs) suppresses the entanglement within the system and thus drives the system to enter the “area law” entanglement phase. We have found that when the power-law decay exponent p is large, i.e., relatively short-range hopping, the entanglement decays to zero fastly with increasing system size in the presence of the measurement, similar to the previous study with the nearest neighbor hopping [40]. On the other hand, when the power-law decay exponent p is small, we have found that the effect of long-range hopping dominates and observed an algebraic scaling for entanglement with the system size accessible in this work. However, as indicated by the local density distribution and classical entropy, we have shown that the systems ultimately enter the skin effect induced “area law” entanglement phase in the thermodynamic limit. Moreover, we have demonstrated that conditional feedback is still necessary for the measurement-induced skin effect with long-range hopping. Although the numerical results are sensitive to the time step δt . We further proved the existence of a “pseudo skin effect” for the case without

conditional feedback.

In principle, the all-to-all hopping, i.e., the $p \rightarrow 0$ limit, can suppress the skin effect and may sustain large-scale entanglement. One interesting direction for future work is to explore other long-range hopping models which may exhibit the measurement-induced entanglement phase transition. In addition, the many-body interaction is unavoidable for natural physical systems. Another interesting direction is to explore the competition between skin effect and long-range interaction.

ACKNOWLEDGMENTS

We thank Yupeng Wang and Jie Ren for the valuable discussions. This work was supported by the National Natural Science Foundation of China under Grant No. 12175015 and No. 11734002. The authors acknowledge the support extended by the Super Computing Center of Beijing Normal University.

-
- [1] B. Skinner, J. Ruhman, and A. Nahum, Measurement-induced phase transitions in the dynamics of entanglement, *Phys. Rev. X* **9**, 031009 (2019).
 - [2] Y. Li, X. Chen, and M. P. A. Fisher, Quantum zeno effect and the many-body entanglement transition, *Phys. Rev. B* **98**, 205136 (2018).
 - [3] Y. Li, X. Chen, and M. P. A. Fisher, Measurement-driven entanglement transition in hybrid quantum circuits, *Phys. Rev. B* **100**, 134306 (2019).
 - [4] A. Chan, R. M. Nandkishore, M. Pretko, and G. Smith, Unitary-projective entanglement dynamics, *Phys. Rev. B* **99**, 224307 (2019).
 - [5] M. Ippoliti and V. Khemani, Postselection-free entanglement dynamics via spacetime duality, *Phys. Rev. Lett.* **126**, 060501 (2021).
 - [6] S. Liu, M.-R. Li, S.-X. Zhang, S.-K. Jian, and H. Yao, Universal KPZ scaling in noisy hybrid quantum circuits, [arXiv:2212.03901](https://arxiv.org/abs/2212.03901) (2022), [10.48550/arXiv.2212.03901](https://arxiv.org/abs/10.48550/arXiv.2212.03901).
 - [7] M. Ippoliti, T. Rakovszky, and V. Khemani, Fractal, logarithmic, and volume-law entangled nonthermal steady states via spacetime duality, *Phys. Rev. X* **12**, 011045 (2022).
 - [8] T.-C. Lu and T. Grover, Spacetime duality between localization transitions and measurement-induced transitions, *PRX Quantum* **2**, 040319 (2021).
 - [9] M. Szyniszewski, A. Romito, and H. Schomerus, Entanglement transition from variable-strength weak measurements, *Phys. Rev. B* **100**, 064204 (2019).
 - [10] S. Choi, Y. Bao, X.-L. Qi, and E. Altman, Quantum error correction in scrambling dynamics and measurement-induced phase transition, *Phys. Rev. Lett.* **125**, 030505 (2020).
 - [11] M. J. Gullans and D. A. Huse, Dynamical purification phase transition induced by quantum measurements, *Phys. Rev. X* **10**, 041020 (2020).
 - [12] Y. Bao, S. Choi, and E. Altman, Theory of the phase transition in random unitary circuits with measurements, *Phys. Rev. B* **101**, 104301 (2020).
 - [13] R. Fan, S. Vijay, A. Vishwanath, and Y.-Z. You, Self-organized error correction in random unitary circuits with measurement, *Phys. Rev. B* **103**, 174309 (2021).
 - [14] Y. Li and M. P. A. Fisher, Statistical mechanics of quantum error correcting codes, *Phys. Rev. B* **103**, 104306 (2021).
 - [15] C.-M. Jian, Y.-Z. You, R. Vasseur, and A. W. W. Ludwig, Measurement-induced criticality in random quantum circuits, *Phys. Rev. B* **101**, 104302 (2020).
 - [16] X. Cao, A. Tilloy, and A. D. Luca, Entanglement in a fermion chain under continuous monitoring, *SciPost Phys.* **7**, 024 (2019).
 - [17] O. Alberton, M. Buchhold, and S. Diehl, Entanglement transition in a monitored free-fermion chain: From extended criticality to area law, *Phys. Rev. Lett.* **126**, 170602 (2021).
 - [18] X. Turkeshi, A. Biella, R. Fazio, M. Dalmonte, and M. Schiró, Measurement-induced entanglement transitions in the quantum ising chain: From infinite to zero clicks, *Phys. Rev. B* **103**, 224210 (2021).
 - [19] X. Turkeshi, M. Dalmonte, R. Fazio, and M. Schiró, Entanglement transitions from stochastic resetting of non-hermitian quasiparticles, *Phys. Rev. B* **105**, L241114 (2022).
 - [20] A. Biella and M. Schiró, Many-Body Quantum Zeno Effect and Measurement-Induced Subradiance Transition, *Quantum* **5**, 528 (2021).
 - [21] G. Piccitto, A. Russomanno, and D. Rossini, Entanglement transitions in the quantum ising chain: A comparison between different unravelings of the same lindbladian, *Phys. Rev. B* **105**, 064305 (2022).
 - [22] M. Buchhold, Y. Minoguchi, A. Altland, and S. Diehl, Effective theory for the measurement-induced phase transition of dirac fermions, *Phys. Rev. X* **11**, 041004 (2021).
 - [23] G. Kells, D. Meidan, and A. Romito, Topological transitions with continuously monitored free fermions, (2021),

- 10.48550/ARXIV.2112.09787.
- [24] M. Block, Y. Bao, S. Choi, E. Altman, and N. Y. Yao, Measurement-induced transition in long-range interacting quantum circuits, *Phys. Rev. Lett.* **128**, 010604 (2022).
- [25] T. Müller, S. Diehl, and M. Buchhold, Measurement-induced dark state phase transitions in long-ranged fermion systems, *Phys. Rev. Lett.* **128**, 010605 (2022).
- [26] T. Minato, K. Sugimoto, T. Kuwahara, and K. Saito, Fate of measurement-induced phase transition in long-range interactions, *Phys. Rev. Lett.* **128**, 010603 (2022).
- [27] S. Yao and Z. Wang, Edge states and topological invariants of non-hermitian systems, *Phys. Rev. Lett.* **121**, 086803 (2018).
- [28] L. Xiao, T. Deng, K. Wang, G. Zhu, Z. Wang, W. Yi, and P. Xue, Non-hermitian bulk–boundary correspondence in quantum dynamics, *Nature Physics* **16**, 761 (2020).
- [29] K. Zhang, Z. Yang, and C. Fang, Correspondence between winding numbers and skin modes in non-hermitian systems, *Phys. Rev. Lett.* **125**, 126402 (2020).
- [30] N. Okuma, K. Kawabata, K. Shiozaki, and M. Sato, Topological origin of non-hermitian skin effects, *Phys. Rev. Lett.* **124**, 086801 (2020).
- [31] C. H. Lee and R. Thomale, Anatomy of skin modes and topology in non-hermitian systems, *Phys. Rev. B* **99**, 201103 (2019).
- [32] D. S. Borgnia, A. J. Kruchkov, and R.-J. Slager, Non-hermitian boundary modes and topology, *Phys. Rev. Lett.* **124**, 056802 (2020).
- [33] K. Yokomizo and S. Murakami, Non-bloch band theory of non-hermitian systems, *Phys. Rev. Lett.* **123**, 066404 (2019).
- [34] Z. Yang, K. Zhang, C. Fang, and J. Hu, Non-hermitian bulk-boundary correspondence and auxiliary generalized brillouin zone theory, *Phys. Rev. Lett.* **125**, 226402 (2020).
- [35] C.-X. Guo, C.-H. Liu, X.-M. Zhao, Y. Liu, and S. Chen, Exact solution of non-hermitian systems with generalized boundary conditions: Size-dependent boundary effect and fragility of the skin effect, *Phys. Rev. Lett.* **127**, 116801 (2021).
- [36] L. Li, C. H. Lee, S. Mu, and J. Gong, Critical non-hermitian skin effect, *Nature communications* **11**, 1 (2020).
- [37] E. J. Bergholtz, J. C. Budich, and F. K. Kunst, Exceptional topology of non-hermitian systems, *Rev. Mod. Phys.* **93**, 015005 (2021).
- [38] L.-M. Chen, S. A. Chen, and P. Ye, Entanglement, non-hermiticity, and duality, *SciPost Phys.* **11**, 003 (2021).
- [39] K. Kawabata, T. Numasawa, and S. Ryu, Entanglement phase transition induced by the non-hermitian skin effect, [arXiv:2206.05384 \[cond-mat.stat-mech\]](https://arxiv.org/abs/2206.05384) (2022), 10.48550/ARXIV.2206.05384.
- [40] J. Ren, Y. Wang, and C. Fang, Measurement-induced skin effect and the absence of entanglement phase transition, [arXiv:2209.11241 \[cond-mat, physics:quant-ph\]](https://arxiv.org/abs/2209.11241) (2022).
- [41] H. M. Wiseman and G. J. Milburn, Quantum measurement and control, (2009), 10.1017/CBO9780511813948.
- [42] K. Jacobs and D. A. Steck, A straightforward introduction to continuous quantum measurement, *Contemporary Physics* **47**, 279 (2006).
- [43] C. Gardiner and P. Zoller, Quantum noise: A handbook of markovian and non-markovian quantum stochastic methods with applications to quantum optics, *Springer Series in Synergetics* (2004).
- [44] A. Barchielli and M. Gregoratti, Quantum trajectories and measurements in continuous time: the diffusive case, *Phys. Rev. Lett.* **77**, 570 (1996).
- [45] H.-P. Breuer and F. Petruccione, The theory of open quantum systems (Oxford University Press, 2007).
- [46] N. Hatano and D. R. Nelson, Localization transitions in non-hermitian quantum mechanics, *Phys. Rev. Lett.* **77**, 570 (1996).
- [47] F. Alsallom, L. Herviou, O. V. Yazyev, and M. Brzezińska, Fate of the non-hermitian skin effect in many-body fermionic systems, *Phys. Rev. Research* **4**, 033122 (2022).
- [48] P. Calabrese and J. Cardy, Evolution of entanglement entropy in one-dimensional systems, *Journal of Statistical Mechanics: Theory and Experiment* **2005**, P04010 (2005).
- [49] A. R. Its, B.-Q. Jin, and V. E. Korepin, Entanglement in the xy spin chain, *Journal of Physics A: Mathematical and General* **38**, 2975 (2005).
- [50] I. Peschel and V. Eisler, Reduced density matrices and entanglement entropy in free lattice models, *Journal of Physics A: Mathematical and Theoretical* **42**, 504003 (2009).
- [51] I. Peschel, On the entanglement entropy for an xy spin chain, *Journal of Statistical Mechanics: Theory and Experiment* **2004**, P12005 (2004).
- [52] I. Peschel, Calculation of reduced density matrices from correlation functions, *Journal of Physics A: Mathematical and General* **36**, L205 (2003).
- [53] M. A. Nielsen and I. L. Chuang, Quantum computation and quantum information: 10th anniversary edition (Cambridge University Press, 2010).
- [54] H. Araki and E. H. Lieb, Entropy inequalities, *Communications in Mathematical Physics* **18**, 160 (1970).
- [55] G. Lindblad, On the generators of quantum dynamical semigroups, *Communications in Mathematical Physics* **48**, 119 (1976).
- [56] F. Yang, Q.-D. Jiang, and E. J. Bergholtz, Liouvillian skin effect in an exactly solvable model, *Phys. Rev. Res.* **4**, 023160 (2022).
- [57] A. J. Daley, Quantum trajectories and open many-body quantum systems, *Advances in Physics* **63**, 77 (2014).

Appendix A: Details to simulate single trajectory and averaged trajectories dynamics

Since the evolution equation (Eq. 2) is quadratic, if the initial state is Gaussian, it will preserve gaussianity through evolution. Assume the system size is L , particle number is N , for free fermions, state $|\psi\rangle$ can be written as $|\psi\rangle = \prod_{i=1}^N (\sum_{j=1}^L U_{ji}(t) c_j^\dagger) |0\rangle$. $|\psi\rangle$ is a Slater determinant state of N fermions, where the columns of U give the single-particle wave functions. The state $|\psi\rangle$ can be simply represented by $L \times N$ matrix $|U\rangle$. Physically, the state will keep invariant with elementary column operations.

To simulate the stochastic Schrodinger equation (Eq. 2), it's easy to prove in the first order approximation of δt , the Eq. 2 is equivalent to

$$|\psi(t + \delta t)\rangle = dW_n \hat{L}_n \frac{e^{-i\hat{H}_{\text{eff}}\delta t} |\psi(t)\rangle}{\|\hat{L}_n e^{-i\hat{H}_{\text{eff}}\delta t} |\psi(t)\rangle\|} + (1 - dW_n) \frac{e^{-i\hat{H}_{\text{eff}}\delta t} |\psi(t)\rangle}{\|e^{-i\hat{H}_{\text{eff}}\delta t} |\psi(t)\rangle\|}, \quad (\text{S1})$$

in which $dW_n = \gamma \langle L_n^\dagger L_n \rangle \delta t$. Physically, the Eq. S1 is in accordance with quantum trajectory theory [57], the state will evolve under effective non-Hermitian Hamiltonian in a short time, then undergo possible quantum jumps and so on.

1) non-Hermitian evolution

$$|\psi(t + \delta t)\rangle = e^{-i\hat{H}_{\text{eff}}\delta t} |\psi(t)\rangle = \prod_{i=1}^N (\sum_{j=1}^L U_{ji}(t) e^{-i\hat{H}_{\text{eff}}\delta t} c_j^\dagger e^{i\hat{H}_{\text{eff}}\delta t}) |0\rangle, \quad (\text{S2})$$

Assume $\hat{H}_{\text{eff}} = \sum_{m,n} h_{\text{eff}}^{mn} \hat{c}_m^\dagger \hat{c}_n$, using Baker–Campbell–Hausdorff formula, we can get,

$$\begin{aligned} e^{-i\hat{H}_{\text{eff}}\delta t} c_j^\dagger e^{i\hat{H}_{\text{eff}}\delta t} &= \sum_{m=1}^L [e^{-ih_{\text{eff}}\delta t}]_{m,j} c_m^\dagger, \\ &= \prod_{i=1}^N (\sum_{j=1}^L U_{ji}(t) \sum_{m=1}^L [e^{-ih_{\text{eff}}\delta t}]_{m,j} c_m^\dagger) |0\rangle \\ &= \prod_{i=1}^N \sum_{m=1}^L [e^{-ih_{\text{eff}}\delta t}]_{m,i} c_m^\dagger |0\rangle, \end{aligned} \quad (\text{S3})$$

In a word, $U(t + \delta t) = e^{-ih_{\text{eff}}\delta t} U(t)$. To preserve $U^\dagger U = I$, we can make QR decomposition, $U(t + \delta t) = Q \cdot R$, and reassign $U(t + \delta t)$ as Q

2) Next, consider the action of quantum jumps

$$U(t + \delta t) \rangle = M_{\delta t} [e^{-iH_{\text{eff}}\delta t} |U(t)\rangle], \quad M_{\delta t} [|U\rangle] = \prod_{i \in P} \frac{L_i |U\rangle}{\|L_i |U\rangle\|}, \quad (\text{S4})$$

where $P = \{n | r_n < \gamma \langle L_n^\dagger L_n \rangle \delta t\}$, $r_n \in (0, 1)$ is a set of independent random variables. In detail, after the non-Hermitian evolution, we can generate a

set of random numbers r_n to decide whether quantum jump \hat{L}_n will happen. Assume $\hat{L}_i = e^{i\pi \hat{n}_{i+1}} \hat{\xi}_i^\dagger \hat{\xi}_i$, $\hat{\xi}_i^\dagger = \sum_k a_{ik} \hat{c}_k$, the probability of the quantum jump \hat{L}_i is $p_i = \langle \psi | \hat{L}_i^\dagger \hat{L}_i | \psi \rangle \gamma \delta t = \langle \psi | \hat{\xi}_i^\dagger \hat{\xi}_i | \psi \rangle \gamma \delta t = \|\hat{\xi}_i | \psi \rangle\|^2 \gamma \delta t$

$$\begin{aligned} \hat{\xi}_i | \psi \rangle &= (\sum_k a_{ik}^* \hat{c}_k) \prod_{i=1}^N (\sum_{j=1}^L U_{jl}(t) c_j^\dagger) |0\rangle \\ &= \sum_i \langle a | U_i \rangle \otimes_{j \neq i} |U_j\rangle, \end{aligned} \quad (\text{S5})$$

Because of $U^\dagger U = I$, we can get $p_i = \sum_i |\langle a | U_i \rangle|^2$. To simplify the expression, remember that the state is invariant for the elementary column operations, we can pre-orthogonalize, find the first column i which satisfies $\langle a | U_i \rangle \neq 0$, then move the column i into the first column, and transform the left columns as

$$|U'_j\rangle = |U_j\rangle - \frac{\langle a | U_j \rangle}{\langle a | U_1 \rangle} |U_1\rangle, \quad (\text{S6})$$

So $\forall j \geq 2$, $\langle a | U'_j \rangle = 0$, and $\hat{\xi}_i | \psi \rangle = \otimes_{i \geq 2} |U'_i\rangle$. After the action of Lindblad operator, $\hat{L}_i | \psi \rangle = e^{i\pi \hat{n}_{i+1}} \hat{\xi}_i^\dagger \hat{\xi}_i | \psi \rangle = e^{i\pi \hat{n}_{i+1}} [|a\rangle \otimes_{i \geq 2} |U'_i\rangle] = |e^{i\pi M} a\rangle \otimes_{i \geq 2} |e^{i\pi M} U'_i\rangle$, in which M is $L \times L$ matrix, with only one nonzero element $M_{i+1, i+1} = 1$. After the action of quantum jump \hat{L}_i , perform the QR decomposition, and reassign U as Q .

Appendix B: Numerical results

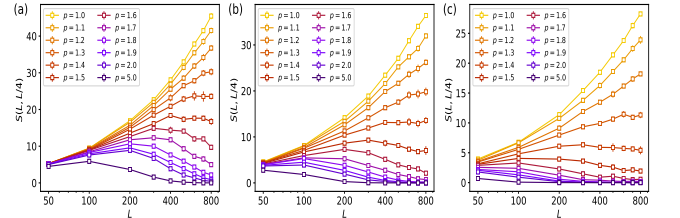


FIG. S1. Entanglement entropy $S(L, L/4)$. (a) $\gamma = 0.05$, (b) $\gamma = 0.1$, (c) $\gamma = 0.2$. With the decrease of p , the hopping range is extended, hence, the skin effect gets weaker and entanglement entropy improves. With the increase of monitoring rate γ , the skin effect gets stronger and entanglement entropy lowers down.

As shown in Fig. S1, for fixed monitoring rate γ , with the decrease of p , namely hopping range getting extended, entanglement entropy grows. Moreover, the threshold L_0 , in which entanglement entropy begins to decay, also increases. While for fixed p , with the increase of monitored rate γ , the skin effect gets stronger, thus entanglement entropy lowers down, and the threshold L_0 also decreases. Worth to mention, for $p = 1.0, 1.1, 1.2$, although entanglement entropy always increases with system size L , however, in the main text, we have pointed

out it's a finite-size effect. To observe the decaying behavior of entanglement entropy for small p , the results with larger system sizes L are required, which is beyond our numerical capabilities.

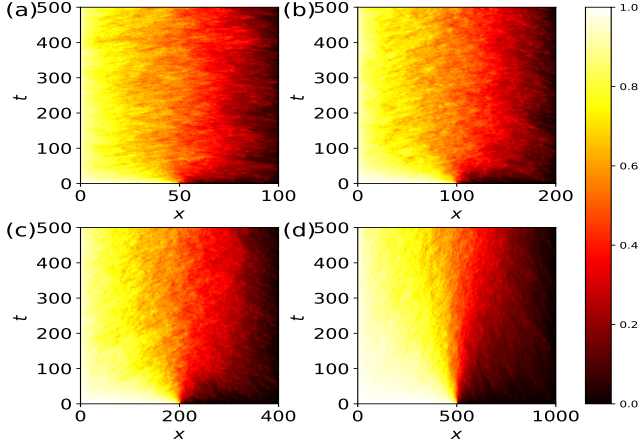


FIG. S2. Density distribution evolution with time. The initial state is chosen as $|111..000\rangle$. $p = 1.1, \gamma = 0.2$, with increasing of system size L ((a) $L = 100$, (b) $L = 200$, (c) $L = 400$, (d) $L = 1000$), fluctuation areas with respect to system size L seem to narrow down

As Fig. S2 shows, for $p = 1.1$ and $\gamma = 0.2$, with the increase of system size L , the ratio of fluctuation areas' size to system size L tends to decrease. Therefore, we predict in the thermodynamical limit, the size of fluctuation areas will saturate, and entanglement entropy obeys "area law". For finite sizes we calculate, even for $L = 1000$, the fluctuation areas' size is still comparable with the system size L and always grows with L , which explains why entanglement entropy grows with L all along in Fig. S1 for p close to 1. However, as shown in Fig. 8(b), for $p = 1.1$ and $\gamma = 0.2$, Δn grows with L , which means the skin effect gets strengthened.

Comparing the above pictures with the bottom pic-

tures in Fig. S3, it's clear that the extended hopping range greatly improves the size of fluctuation areas. For $p = 2$, the density distributions are very close to $p = \infty$ case [40], which show the extremely strong skin effect with almost one-half occupied and one-half unoccupied. As for $p = 1.1$ and small γ , when system size L is about $O(10^2)$, fluctuation areas' size is comparable with L . Therefore, entanglement entropy for $p = 2.0$ quickly decays to zero with the increase of L , while for $p = 1.1$ and small γ , at least for $L \leq 800$ entanglement entropy always grows with L (Fig. S1).

For the case without feedback, from Lindblad master equation we know there is no skin effect in steady state, which is demonstrated in Fig. S4. For relatively small $\gamma = 0.4$, time step $\delta t = 0.05$, we can already see the steady state's density distribution is uniform.

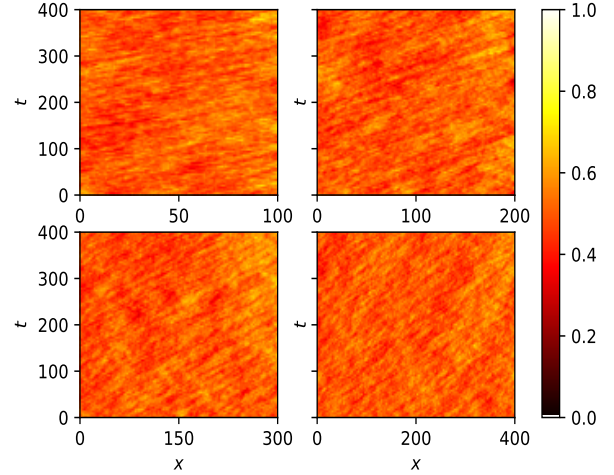


FIG. S4. Density distribution evolution with time without feedback under OBC. The initial state is chosen as $|1010..010\rangle$. For $p = 2.0, \gamma = 0.4$, time step $\delta t = 0.05$ and various sizes L , density distributions are uniform.

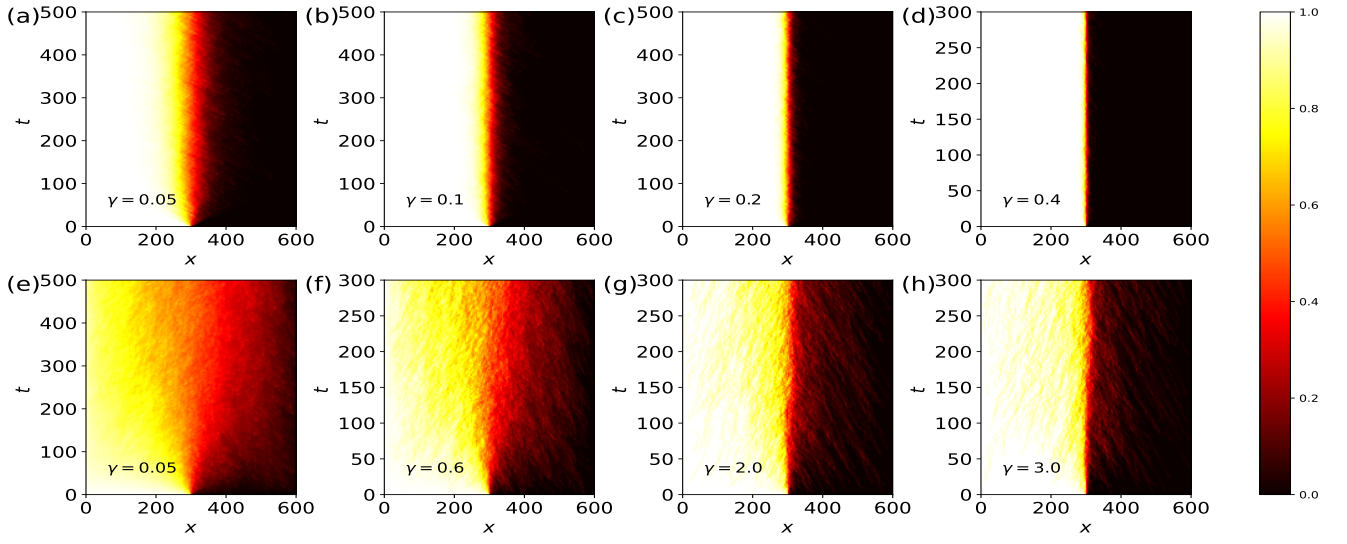


FIG. S3. Density distribution evolution with time. The initial state is chosen as $|111..000\rangle$. above: $p = 2.0$, bottom: $p = 1.1$, for $p = 2.0$, fluctuation areas are small; for $p = 1.1$, longer-range hopping greatly extends fluctuation areas. Both $p = 1.1$ and $p = 2.0$ show that the skin effect is strengthened with the increase of γ .